

Liquid state properties from first principles DFT calculations: Static properties

Nicolas Bock,^{1,*} Erik Holmström,^{2,1} Travis B. Peery,¹ Raquel Lizárraga,^{2,1}

Eric D. Chisolm,¹ Giulia De Lorenzi-Venneri,¹ and Duane C. Wallace¹

¹Theoretical Division, Los Alamos National Laboratory, Los Alamos, NM, 87545

²Instituto de Física, Facultad de Ciencias, Universidad Austral de Chile, Casilla 567, Valdivia, Chile

(Dated: June 21, 2018)

In order to test the vibration-transit (V-T) theory of liquid dynamics, *ab initio* density functional theory (DFT) calculations of thermodynamic properties of Na and Cu are performed and compared with experimental data. The calculations are done for the crystal at $T = 0$ and T_m , and for the liquid at T_m . The key theoretical quantities for crystal and liquid are the structural potential and the dynamical matrix, both as functions of volume. The theoretical equations are presented, as well as details of the DFT computations. The properties compared with experiment are the equilibrium volume, the isothermal bulk modulus, the internal energy and the entropy. The agreement of theory with experiment is uniformly good. Our primary conclusion is that the application of DFT to V-T theory is feasible, and the resulting liquid calculations achieve the same level of accuracy as does *ab initio* lattice dynamics for crystals. Moreover, given the well established reliability of DFT, the present results provide a significant confirmation of V-T theory itself.

PACS numbers: 05.70.Ce, 64.10.+h

I. INTRODUCTION

The goal of our work is to investigate, and to improve where possible, the theoretical procedures for calculating statistical mechanical properties of condensed matter systems. Here we shall focus on elemental crystals and liquids. For many such systems, *ab initio* density functional theory (DFT) provides highly accurate results for the groundstate energy as function of the nuclear positions. This energy is the groundstate adiabatic potential, which appears in the nuclear motion Hamiltonian. For crystals, the nuclear motion Hamiltonian is prescribed by lattice dynamics theory [1]. Thermodynamic properties of elemental crystals, as calculated from DFT together with phonon statistical mechanics, can be nearly as accurate as the experimental measurements. For liquids, in the absence of a tractable nuclear motion Hamiltonian, statistical mechanical properties are calculated from *ab initio* molecular dynamics (MD). These calculations are based on DFT, and can be evaluated in the groundstate adiabatic approximation [2, 3]. Again the results compare very well with experiment. Moreover, the studies reveal detailed characteristics of the electronic structure, for example for liquid Al [4], for liquid Fe [5, 6], and for group III B - VI B elemental liquids [7].

In recent years, vibration-transit (V-T) theory has been under development to provide a tractable approximate Hamiltonian for monatomic liquids [8, 9]. In this theory the nuclear motion is composed of two parts, the many-body vibrational motion in one potential energy valley, plus transits, which carry the system from valley to valley. Transits proceed at a high rate throughout the liquid, and are responsible for diffusion. The

vibrational motion is tractable and is subject to *ab initio* evaluation. Closed-form equations are available for the dominant structural and vibrational contributions to thermodynamic functions. The transit contribution is complicated but small, and is treated by a model. The question we ask is simple and direct: If we apply DFT in the adiabatic approximation to V-T theory, how do the calculated thermodynamic properties compare with experiment? Our purpose here is to provide an initial answer to this question.

The study is done for Na and Cu. The properties we calculate are the equilibrium volume, the isothermal bulk modulus, and the internal energy and entropy. Comparison of theory and experiment is done for the crystal at $T = 0$ and at the melting temperature T_m , and for the liquid at T_m . The crystal tests are made to establish a fiducial for the theoretical accuracy. Both Na and Cu have a nearly-free-electron density of states in the vicinity of the Fermi energy. Hence the electronic excitation contribution to thermodynamic properties is very small and may be calculated from free electron theory. In this way, the ultimate comparison of theory and experiment is not significantly contaminated by error from electronic excitation. On the other hand, while Na has a rigid core, with only one valence electron that deforms as the nucleus moves, both the valence *s*-electron and the filled *d*-shell deform as the nucleus moves in Cu. This strong difference in the groundstate adiabatic potential adds dimension to the present study. While this study is limited to two liquid metals, extensive analysis of experimental data reveal a common behavior of most elemental liquids [8], and Na and Cu are representative of this common behavior.

Before completing the work reported here, two preliminary results were required. First, an efficient DFT quench procedure for locating the many-body potential energy minima was developed [10, 11]. Second, an accu-

*Electronic address: nbock@lanl.gov

rate predictive model for the transit contribution to thermodynamic functions was constructed [12]. The culmination of the complete project is reported here. It must be observed that the present work is not intended to replace *ab initio* MD calculations; indeed the two methods are quite complementary, as discussed in the final section.

In Sec. II, we outline the theory and explain various issues relevant to real-world calculations. In Sec. III, the DFT calculations are described, including quench procedures and the total energy for crystal and liquid structures. (Miscellaneous details related to these sections are collected in the appendices.) Results are presented and discussed in Sec. IV. Intermediate theoretical results show the relative importance of the separate theoretical contributions to internal energy and entropy. Theory and experiment are tabulated and compared at the precision of the experimental accuracy. Conclusions are summarized in Sec. V. The primary conclusion regards the overall accuracy of the present calculations of thermodynamic properties of liquid Na and Cu. A secondary conclusion summarizes the verification of V-T theory which is provided by the present calculations.

II. THEORETICAL FORMULATION

The condensed matter potential energy surface is composed of intersecting many-atom potential energy valleys. Each valley makes a contribution to the partition function. To approximate the single valley partition function, the valley potential is harmonically extended to infinity. The partition function is then simple, at the cost of neglecting anharmonicity and valley-valley intersections. We summarize the harmonic single valley statistical mechanical formulas in Appendix A. In this section we show why these formulas are needed for the present work.

For liquids, the starting point of V-T theory is a hypothesis about the nature of the many-body potential energy valleys which underlie the nuclear motion. These valleys are divided into two classes, random and symmetric. In the thermodynamic limit, the random valleys are supposed to dominate the liquid statistical mechanics, and are also supposed to be macroscopically uniform. Macroscopic uniformity means that the statistical mechanical average of any macroscopic dynamical variable is the same for all random valleys. Therefore the vibrational contribution to a thermodynamic function can be calculated from a single random valley harmonically extended to infinity. The single-valley vibrational motion is supposed to be interspersed with transits, which carry the system from valley to valley. Hence there are two separate components of the nuclear motion, vibrations and transits. With a superscript l to represent the liquid, the total free energy $F^l(V, T)$ is written

$$F^l(V, T) = \Phi_0^l(V) + F_{\text{vib}}^l(V, T) + F_{\text{tr}}^l(V, T) + F_{\text{el}}^l(V, T). \quad (1)$$

Here $\Phi_0^l(V)$ is the system potential energy at the random valley structure, and $F_{\text{vib}}^l(V, T)$ and $F_{\text{tr}}^l(V, T)$ ex-

press respectively the nuclear motion contribution from vibrations and transits. The final term, $F_{\text{el}}^l(V, T)$, represents electronic excitations; it is added here because Na and Cu, the materials we study, are metals. However, $F_{\text{el}}^l(V, T)$ is very small, and free-electron theory in the leading Sommerfeld expansion provides sufficient accuracy.

The corresponding internal energy $U^l(V, T)$ and entropy $S^l(V, T)$ are

$$U^l(V, T) = \Phi_0^l(V) + U_{\text{vib}}^l(V, T) + U_{\text{tr}}^l(V, T) + U_{\text{el}}^l(V, T), \quad (2)$$

$$S^l(V, T) = S_{\text{vib}}^l(V, T) + S_{\text{tr}}^l(V, T) + S_{\text{el}}^l(V, T). \quad (3)$$

At $T \geq T_m$, the melting temperature, the high- T expansions Eqs. (A10) and (A11) are valid, hence the primary potential energy parameters are $\Phi_0^l(V)$ for the internal energy and $\theta_0^l(V)$ for the entropy. $\theta_0^l(V)$ is the characteristic temperature related to the log moment of the vibrational spectrum (see Appendix A).

A new challenge, unique to the liquid, is to find the structures corresponding to random valleys so the characteristic functions may be calculated. The technique we've developed to do so [10, 11] exploits their numerical dominance; we start with computer generated *stochastic* configurations, in which the nuclei are distributed uniformly over the system volume, within a constraint limiting the closeness of approach of any pair. As we demonstrate in [10, 11], quenching from such a configuration lands the system in a random valley with high likelihood.

Once the structure is found, the system potential is corrected to the thermodynamic zero to produce $\Phi_0^l(V)$ (see Appendix B). The dynamical matrix is the mass-weighted curvature tensor evaluated at the structure. This is calculated by a finite-difference approach in which each individual nucleus is displaced in all three Cartesian directions and the forces on all nuclei are computed. The eigenvalues are $M\omega_\lambda^2$ for $\lambda = 1, \dots, 3N$, where M is the nuclear mass and ω_λ are the normal mode vibrational frequencies. Here, to calculate thermodynamic functions, only the eigenvalues are needed. However, the eigenvectors are also important, as they are needed to calculate fluctuations and time correlation functions [13].

Although we will perform these calculations in Sec. III using periodic boundary conditions, that does not imply that the liquid vibrations correspond to those of a crystal with a large unit cell. The liquid vibrational modes are fundamentally different from those of a crystal. Since a crystal is periodic in space, periodic boundary conditions on a crystal unit cell or supercell merely express the infinite extension of the crystal. This is the infinite lattice model [1], and entails no error. A liquid is represented by a random structure, which has no spatial periodicity, and calculations for a finite system contain surface errors. Such errors are minimized by the application of periodic boundary conditions, but the resulting spatial periodicity is not physically correct or meaningful for the liquid.

TABLE I: Transit contributions to energy and entropy at melt. [12]

Element	T_m/θ_{tr}	$U_{\text{tr}}/Nk_B T_m$	S_{tr}/Nk_B
Na	0.65	0.415	0.72
Cu	1.00	0.332	0.80

Finally for the liquid, we must evaluate the transit contributions to the internal energy and entropy at melt. It was just this requirement, in the present application of DFT to liquid dynamics theory, that motivated our development of an improved model for the transit free energy of monatomic liquids. This model consists of two parts: (a) The available high- T experimental entropy data were analyzed in terms of the entropy formulas, Eqs. (3) and (A10), revealing a scaled T -dependence of $S_{\text{tr}}^l(V, T)$ at fixed volume [14], and (b) a statistical mechanical model for $F_{\text{tr}}^l(V, T)$ was calibrated to this experimental $S_{\text{tr}}^l(V, T)$ function, yielding model equations for all thermodynamic functions which derive from the transit free energy [12]. The model provides universal curves for S_{tr}^l/Nk_B and $U_{\text{tr}}^l/Nk_B T$ in terms of $T/\theta_{\text{tr}}(V)$, where $\theta_{\text{tr}}(V)$ is the material-specific scaling temperature for the transit entropy. Results for Na and Cu at melt are listed in Table I. Volume dependence of the transit contribution is neglected.

The temperature $\theta_{\text{tr}}(V)$ plays a role in the transit contribution similar to that played by $\theta_0(V)$ in the vibrational contribution; it sets a material-specific temperature scale. We know how to calculate $\theta_0(V)$ from first principles because the relevant term in the liquid Hamiltonian (the vibrational part) is well-understood; however, the theory for the transit contribution to the Hamiltonian is still under development. Once the transit term is understood, we hope to be able to calculate $\theta_{\text{tr}}(V)$ from first principles as well. For now, parameterization from data will suffice.

In the crystal, the system moves in the crystal potential energy valley, and this motion is well described by lattice dynamics theory [1]. In the harmonic approximation, and neglecting valley-valley intersections, the equations of Appendix A apply. Therefore, the total crystal free energy is

$$F^c(V, T) = \Phi_0^c(V) + F_{\text{vib}}^c(V, T) + F_{\text{el}}^c(V, T), \quad (4)$$

where $\Phi_0^c(V)$ is the system potential at the valley minimum, the crystal structure, and $F_{\text{vib}}^c(V, T)$ is the contribution from lattice vibrations. Again the electronic excitation term $F_{\text{el}}^c(V, T)$ is very small and is given to sufficient accuracy by free electron theory.

Corresponding to Eq. (4), the crystal internal energy and entropy are given by

$$U^c(V, T) = \Phi_0^c(V) + U_{\text{vib}}^c(V, T) + U_{\text{el}}^c(V, T), \quad (5)$$

$$S^c(V, T) = S_{\text{vib}}^c(V, T) + S_{\text{el}}^c(V, T). \quad (6)$$

TABLE II: Setup parameters for the VASP calculations. The Monkhorst-Pack \mathbf{k} -mesh is recorded as $[n, n, n]$, followed by the number of \mathbf{k} -points in the irreducible Brillouin zone as ($n_{\mathbf{k}}$). The quantity “translational invariance” is the maximum magnitude of translational eigenvalues relative to that of the lowest pure vibrational mode. “DM” is short for “dynamical matrix.”

Quantity	Na	Cu
valence electrons	1	11
planewave cutoff [eV]	101.7	341.6
max core radius [\AA]	2.5	2.3
EDIFF [eV]	10^{-8}	10^{-8}
\mathbf{k} -mesh for $E^l(V)$	[3, 3, 3] (14)	[5, 5, 5] (63)
\mathbf{k} -mesh for liquid DM	[3, 3, 3] (14)	[2, 2, 2] (4)
translational invariance (liquid)	10^{-6}	10^{-6}
crystal structure	bcc	fcc
\mathbf{k} -mesh for crystal DM	[3, 3, 3] (10)	[2, 2, 2] (2)
translational invariance (crystal)	10^{-13}	10^{-7}

For Na and Cu, as with most elements, the high- T expansions Eqs. (A10) and (A11) are accurate at T_m for the crystal as well as the liquid. The fundamental differences in finite- N errors for crystal and liquid are described in the following Section.

III. ELECTRONIC STRUCTURE CALCULATIONS

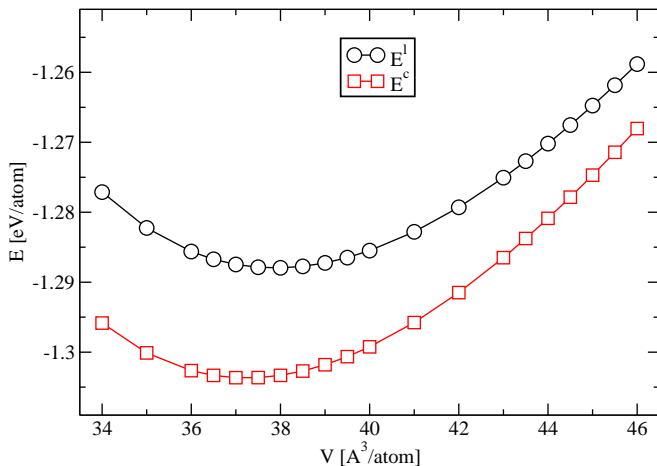
A. Calculations for the liquid

Our supercell consists of 150 atoms in a cubic box with periodic boundary conditions. The value $N = 150$ is large enough that finite- N errors are not serious, and small enough that a sufficient number of total energy calculations (a few thousand) can be done for each element.

The DFT calculations are done with the VASP code [15], using the projector augmented wave (PAW) method [16] in the generalized gradient approximation (GGA) [17]. The \mathbf{k} -point mesh was automatically generated using the method of Monkhorst and Pack [18]. The setup parameters are listed in Table II. It is the large size of the real-space supercell which allows us to use few \mathbf{k} -points in comparison to the large number (several thousands) needed for crystal metal calculations with small unit cells.

To locate structures, we followed the procedure outlined in Sec. II [10, 11]. A quench is considered converged when the energy decrease in one iteration is less than 10 times the current EDIFF setting, where EDIFF defines the energy convergence criterion used in the SCF procedure (see Table II). Initially, quenches were done from a separate stochastic configuration at each volume. To save computer time we quenched to one structure,

FIG. 1: For Na at $N = 150$: DFT results for the structural energy E versus volume V for the liquid (E^l), and for the crystal (E^c).



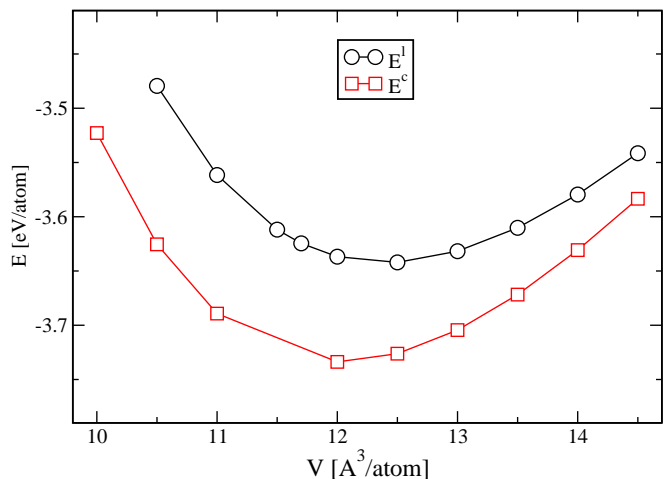
then scaled this structure to slightly larger and smaller volumes, and quenched these configurations to new structures. This was repeated until the desired range of volumes was covered. In quenching with DFT, the following procedure saves computer time: quench to convergence at Monkhorst-Pack \mathbf{k} -mesh [1, 1, 1], then take Monkhorst-Pack \mathbf{k} -mesh [2, 2, 2] and quench to convergence again, and so on. This is faster, not because it requires fewer quench steps, but because most of the steps are at a smaller number of \mathbf{k} -points.

The DFT energy of a random structure is denoted $E^l(V)$. The results for Na and Cu are shown in Figs. 1 and 2 respectively. The crystal structure energies $E^c(V)$ are also shown in the figures. From the potential energy hypothesis mentioned in Sec. II, for a given element at a given V , the random structural energies should occupy a distribution whose width is small compared to $k_B T_m$, and whose mean lies above E^c by around $k_B T_m$. This characteristic is well verified for Na at the volume V_m^l of the liquid at melt [10, 19, 20]. Here, since each $E^l(V)$ is a representative of the random distribution at that V , the curves of $E^l(V)$ and $E^c(V)$ in Fig. 1 confirm the characteristic random structure distribution over a range of volumes for Na. The same confirmation is provided for Cu in Fig. 2. These energies are then normalized as described in Appendix B to provide the structural potential for the liquid, $\Phi_0^l(V)$.

In the many quenches done in the present study, very few symmetric structures have appeared. These structures invariably have DFT energies lying noticeably below the curve of $E^l(V)$, and above $E^c(V)$. This also accords with the potential energy hypothesis of V-T theory, Sec. II, and accords with previous findings [10, 19, 20] for Na at V_m^l .

For a given liquid at fixed density, the macroscopic random structure is better approximated with an ever larger supercell. Hence at finite N all calculated potential energy parameters will have an error due to finite resolution

FIG. 2: For Cu at $N = 150$: DFT results for the structural energy E versus volume V for the liquid (E^l), and for the crystal (E^c).

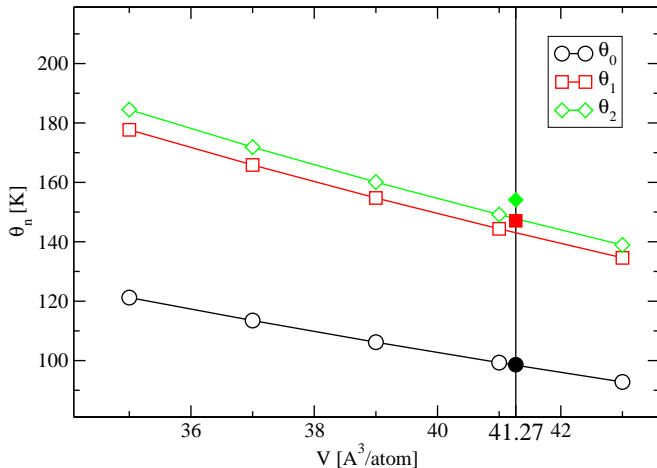


of the structure. Moreover the vibrational characteristic temperatures are subject to a second finite- N error, due to the incomplete resolution of the frequency distribution. This second error is the dominant error in our liquid characteristic temperature calculations.

Among the normal modes are three, $\lambda = 1, 2, 3$, representing uniform translation of the system. Their eigenvalues are in principle zero due to translational invariance (also called the acoustic sum rule in crystal theory). In practice the translational eigenvalues are zero only to numerical accuracy, and are of either sign. The remaining $3N - 3$ modes are pure vibrational and have positive eigenvalues, by the definition of a structure as a local minimum. To check translational invariance, the ratio of eigenvalues $|\omega_\lambda^2|/\omega_4^2$ is calculated for $\lambda = 1, 2, 3$, where mode $\lambda = 4$ is the lowest lying pure vibrational mode. The maximum value of this ratio in our final calculations for each element is listed under the designation “translational invariance” in Table II. The requirement is clearly satisfied to high numerical accuracy.

Here we are interested in moments of the frequency distribution, which are related to characteristic temperatures θ_n by Eqs. (A3) - (A5), where the translational eigenvalues are excluded from the average. Our calculations of these θ_n for Na are shown in Fig. 3. Also shown are values from a well-tested interatomic potential for Na, for a 500 atom system at the volume of the liquid at melt [20]. Agreement is excellent for θ_0 , and is good for θ_1 and θ_2 . It is common for theory and experiment both to give more reliable values for θ_0 than for other θ_n . The reason is that θ_0 , being the log moment, is uniformly sensitive to all ω_λ in the spectrum, while other θ_n are more sensitive to higher (or lower) frequencies, hence depend on a smaller portion of the spectrum.

FIG. 3: For liquid Na at $N = 150$: DFT results for the vibrational characteristic temperatures θ_n versus volume V , for $n = 0, 1, 2$ (open symbols). Also the same θ_n at $N = 500$ and $V = V_m^l$, from Na interatomic potentials [20] (solid symbols).



B. Calculations for the crystal

For the structural energy calculations, we use one primitive unit cell with periodic boundary conditions, and increase the \mathbf{k} -mesh to convergence. This represents the infinite lattice model [1], and there are no finite- N errors. The situation contrasts with the liquid calculation, where the structure itself contains a finite- N error.

For the crystal, our calculated phonon moments can be tested against results from inelastic neutron scattering [21]. This will ultimately allow us to estimate the accuracy of the calculated liquid moments. To this end, we calculate the crystal dynamical matrix for a large supercell with periodic boundary conditions, just as for the liquid. The procedure yields phonons with wavevectors commensurate with the supercell. The crystal structure is precise, but the phonon moments have finite- N error due to the limited resolution of the frequency distribution. Since this is also the major error in the liquid, we expect the total error in vibrational characteristic temperatures to be about the same for crystal and liquid at a given N .

To calculate the dynamical matrix, a rhombohedral supercell of $5 \times 5 \times 5$ primitive unit cells was constructed for bcc and fcc lattices [22]. This gives $N = 125$, as close as possible to the liquid value of N . A fixed \mathbf{k} -mesh was chosen, the same as that used for the liquid; the same \mathbf{k} -mesh produces a smaller number of \mathbf{k} -points in the irreducible Brillouin zone for the crystal (see Table II).

TABLE III: Intermediate Theoretical Results

Quantity	Na	Cu
Crystal at $T = 0$		
V_{ref}^c [$\text{\AA}^3/\text{atom}$]	37.24	12.02
D [eV/atom]	1.28763	3.7047
$\frac{9}{8}Nk_B\theta_1$ [meV/atom]	16.05	29.3
$\frac{9}{8}k_B\theta_1/3k_B T_m$	0.167	0.087
Crystal at T_m		
V_m^c [$\text{\AA}^3/\text{atom}$]	39.79	13.05
Φ_0^c [meV/atom]	-12.22	3.1
U_{vib}^c [meV/atom]	96.72	351.7
U_{el}^c [meV/atom]	0.82	5.3
S_{vib}^c [k_B/atom]	6.79	9.03
S_{el}^c [k_B/atom]	0.05	0.09
Liquid at T_m		
V_m^l [$\text{\AA}^3/\text{atom}$]	40.93	13.54
Φ_0^l [meV/atom]	4.62	96.5
U_{vib}^l [meV/atom]	96.65	351.7
U_{tr}^l [meV/atom]	13.27	38.9
U_{el}^l [meV/atom]	0.82	5.2
S_{vib}^l [k_B/atom]	6.96	9.39
S_{tr}^l [k_B/atom]	0.72	0.80
S_{el}^l [k_B/atom]	0.05	0.09

IV. RESULTS

A. Intermediate theoretical results

For the crystal at $T = 0$ and T_m , and for the liquid at T_m , we fit the four-parameter Vinet-Rose function [23] to our calculated $F(V, T)$ versus V . From this we find the volume at $P = 0$, and the isothermal bulk modulus B at that volume. Intermediate theoretical results calculated from the formulas of Sec. II are listed in Table III. These show the relative importance of various theoretical contributions to internal energy and entropy. The discussion here is for Na and Cu collectively, and is qualitatively applicable to monatomic crystals and liquids in general.

At $T = 0$, the free energy is given by Eqs. (B1) - (B3). For accurate theoretical work, the zero-point energy cannot be neglected. For the light elements the zero-point energy measurably affects the volume at $P = 0$ (see also Ref. [24], Table 16.3). For all elements, the zero-point energy is important in the internal energies of crystal and liquid states. This is shown by the ratio of the zero-point energy to the classical vibrational energy at melt, $\frac{9}{8}k_B\theta_1^c/3k_B T_m$, listed in Table III. If the zero-point energy is omitted from theory, this ratio is the relative error made in the (dominant) internal energy contribution $U_{\text{vib}}(V, T)$.

For the crystal at melt, the internal energy and entropy are given by Eqs. (5) and (6). From Table III, the domi-

nant energy contribution is U_{vib}^c . The small contribution from Φ_0^c is a combination of the volume-dependent part of $E^c(V)$, and the zero-point energy, according to Eqs. (B2) and (B3). The contribution $E^c(V) - E^c(V_{\text{ref}}^c)$ can be read from Figs. 1 and 2. The dominant entropy contribution is again vibrational. At $T \gtrsim T_m$, S_{vib}^c depends almost entirely on $T/\theta_0^c(V)$, from Eq. (A10). In Table III, the electronic contributions are quite small, being $\lesssim 2\%$ for the crystal at melt. These contributions are much larger, say up to 10%, for metals with unfilled d -bands [25].

The liquid thermodynamic functions contain terms analogous to those in the crystal, plus an added contribution from transits, Eqs. (1) - (3) and (B4). For the liquid at melt, the character of contributions from the structural potential Φ_0^l , from vibrations, and from electronic excitations is qualitatively the same as described above for the crystal at melt. Again the contribution from $E^l(V) - E^c(V_{\text{ref}}^c)$ can be read from Figs. 1 and 2. However, the transit contribution in Table III is approximately 10% for the liquid at melt, and is therefore important for an accurate theory. This is the only entry in Table III not obtained from electronic structure calculations. But this term also will be amenable to DFT calculation, as soon as a model for the transit Hamiltonian is developed.

B. Comparison of theory and experiment

Comparison of theory and experiment for the crystal at $T = 0$ and $P = 0$ is listed in Table IV. Differences are expressed in the quantity Δ , defined in general by

$$\Delta = \frac{\text{theory} - \text{expt}}{\text{expt}}. \quad (7)$$

For the crystal volume and bulk modulus, the agreement is excellent, at the customary level for *ab initio* crystal calculations (see e.g. Ref. [24], Tables 16.2 and 16.3).

In Table IV, comparison of $\theta_n^c(V)$ for $n = 0, 1, 2$ is at the experimental volume V_{meas}^c (see Ref. [24], Table 15.1). The experimental error in $\theta_n^c(V_{\text{meas}}^c)$ is estimated to be 0.1 - 0.5% (p. 151 of Ref. [24]). In our experience, lattice dynamics theory in *ab initio* evaluation can account for the experimental θ_n^c to an accuracy around 1% at best. To achieve such accuracy is not our goal here. Accuracy of the *ab initio* θ_n^c in Table IV is quite respectable, with Δ in the range -2% to $+5\%$. Error at this level is a minor effect in the comparison of theory and experiment for the crystal at melt. Moreover, we attribute the theoretical error mainly to small system size ($N = 125$), since the corresponding small number of vibrational modes can only poorly represent the actual crystal frequency distribution. This problem is easily remedied by increasing N .

Comparison of theory and experiment for the crystal at melt, and for the liquid at melt, is listed in Table V. Notice the nuclear motion causes thermal expansion, as seen in the volume at melt. Specifically, V_m^c is larger than

V at the minimum of $E^c(V)$, and V_m^l is larger than V at the minimum of $E^l(V)$, Figs. 1 and 2. The volumes are in excellent agreement with experiment. Also, at this point we can see that the volume errors are systematic: for all three states, the crystal at $T = 0$ and at T_m , and the liquid at T_m , the volume error is -0.01 for Na, and $+0.03$ for Cu. The bulk modulus, being essentially the curvature of $\Phi_0(V)$, for crystal or for liquid, has larger error than the volume itself. Moreover, the experimental and theoretical determinations of B in Table V are *both* subject to significant errors. The agreement of theory and experiment for B is as good as we can expect at T_m .

It remains to discuss the comparison of theory and experiment for the internal energy and entropy at melt, Table V. The errors here are sufficiently small that individual Δ values cannot be interpreted. The mean and standard deviation of Δ for energy and entropy for crystal and liquid states is $\Delta = -0.005 \pm 0.019$. Hence the errors are essentially pure scatter. Contributions to the scatter arise from two major sources, experimental error at the level of 0.005 - 0.010, and computational error due to small system size at the level of 0.01 - 0.02. Additional smaller errors result from the slightly inaccurate theoretical volume, from error in the free-electron model for electronic excitation, and from neglect of electronic excitation-nuclear motion interaction [31, 32]. It follows that the results in Table V for internal energy and entropy at melt are consistent with known errors.

There is one more systematic property of the comparison in Table V that holds separately for each metal. For the bulk modulus, Δ is large and positive and is roughly the same for crystal and liquid, while for each remaining property, Δ is small and approximately the same magnitude for crystal and liquid. The implication is that the liquid theory we study has the same level of accuracy as does lattice dynamics theory for crystals.

V. CONCLUSIONS

A. The present application of DFT to liquid dynamics

Our primary conclusion from the present study is: Using a standard implementation of DFT, as provided by the VASP code, it is possible to make *ab initio* calculations of thermodynamic properties of monatomic liquids. The liquid calculations achieve the same level of accuracy as does *ab initio* lattice dynamics for crystals, the most accurate crystal theory available. This conclusion is validated for Na and Cu, based on the comparisons of theory with experiment listed in Table V. The following discussion adds detail to the primary conclusion.

The comparisons for the liquid in Table V are at zero pressure and temperature T_m . However, we fully expect the agreement of theory and experiment to hold for a wide range of pressures and temperatures, or equivalently, a wide range of volumes and temperatures. The

TABLE IV: Comparison of theory and experiment for the crystal at low T . V_{ref}^c and B^c are at $T = 0$ and $P = 0$. θ_n^c are at V_{meas}^c , the volume of experimental measurement.

Quantity	Na (bcc)			Cu (fcc)		
	Theory	Expt.	Δ	Theory	Expt.	Δ
V_{ref}^c [$\text{\AA}^3/\text{atom}$]	37.24	37.68 ^a	-0.012	12.02	11.70 ^a	0.027
B^c [GPa]	7.76	7.3-7.6 ^b	0.042	138.7	142.0 ^c	-0.023
V_{meas}^c [$\text{\AA}^3/\text{atom}$]	37.98	37.98 ^a	—	11.70	11.70 ^a	—
θ_0^c [K]	111.2	113.3 ^d	-0.019	236.5	225.3 ^d	0.050
θ_1^c [K]	161.7	163 ^d	-0.008	330.2	315 ^d	0.048
θ_2^c [K]	165.8	166 ^d	-0.001	332.5	317 ^d	0.049

^aTables 15.1 and 19.1 of Ref. [24]

^bSee Refs. [26–29]

^cSee Ref. [30]

^dSee Ref. [21] and Tables 15.1 and 19.1 of Ref. [24]

TABLE V: Comparison of theory and experiment for crystal and liquid at T_m

Quantity	Na (bcc)			Cu (fcc)		
	Theory	Expt.	Δ	Theory	Expt.	Δ
<u>Crystal Data</u>						
V^c [$\text{\AA}^3/\text{atom}$]	39.79	40.27 ^a	-0.012	13.05	12.62 ^a	0.034
B^c [GPa]	6.47	5.8 ^b	0.116	97	90 ^c	0.078
U^c [meV/atom]	85.32	89.1 ^d	-0.042	353.1	358.9 ^d	-0.016
S^c [k_B/atom]	6.84	6.93 ^d	-0.013	9.12	8.93 ^d	0.021
<u>Liquid Data</u>						
V^l [$\text{\AA}^3/\text{atom}$]	40.93	41.27 ^a	-0.008	13.54	13.19 ^a	0.027
B^l [GPa]	5.93	5.3 ^e	0.119	85.7	73.6 ^f	0.164
U^l [meV/atom]	115.36	115.9 ^d	-0.005	492.3	492.7 ^d	-0.001
S^l [k_B/atom]	7.73	7.78 ^d	-0.006	10.28	10.09 ^d	0.019

^aTables 19.1 and 21.1 of Ref. [24]

^bSee Ref. [33]

^cSee Ref. [30]

^dSee Ref. [34]

^eSee Refs. [35, 36]

^fSee Ref. [37]

volume dependence is contained in functions calculated by DFT, primarily $\Phi_0^l(V)$ and $\theta_0^l(V)$. We can expect these functions to be as accurate for the compressed liquid as for the liquid at zero pressure. Moreover, at the fixed volume V_m^l , the temperature dependence of the experimental thermodynamic data is accurately accounted for by the equations of Sec. II and Appendix A. This is because those equations, and the experimental data for entropy at high temperatures, were used to calibrate the statistical mechanical model for the transit free energy [14]. Hence the level of agreement between theory and experiment found in Table V should persist to higher pressures and temperatures.

A potentially useful comparison can be made between the present technique and *ab initio* MD. At a given N , *ab initio* MD requires far greater computer resources to calculate a similar set of thermodynamic data. Or, with a fixed computer resource, the present technique can study

a larger system, and hence obtain greater accuracy by reducing finite- N errors. On the other hand, *ab initio* MD data contain both vibrational and transit contributions. Both techniques together can separate the transit and vibrational contributions to statistical mechanical functions. The combined techniques have the potential to reveal the physical nature of transit motion.

What is achieved by making DFT calculations for the crystal at $T = 0$? First, before we can compare theory and experiment for any condensed matter state, it is necessary to adjust the DFT energy calculations to have the thermodynamic zero of energy. This is accomplished by means of Eqs. (B2) and (B3). A second useful result is the confirmation that DFT calculations are accurate for $\Phi_0^c(V)$, and for the characteristic temperatures θ_0^c , θ_1^c , and θ_2^c . This is shown by the comparisons of Table IV. This confirmation lends confidence to similar calculations for the liquid.

What is achieved by comparing theory and experiment for the crystal at T_m ? This comparison is rarely performed in crystal physics research, and is of interest in itself. The comparisons of Table V confirm that the DFT calculations are accurate for $\Phi_0^c(V)$ and $\theta_0^c(V)$, and their volume derivatives. This confirmation shows the level of accuracy which *ab initio* lattice dynamics can achieve for the crystal at melt, and it also lends confidence to the similar calculations for the liquid.

B. Verification of V-T theory

The primary conclusion is based on the comparison of theoretical and experimental data, and uses no condition on the validity of theory. But the well-established reliability of DFT calculations supports a secondary conclusion regarding the theory itself. The theory consists of two parts, the V-T equations and DFT calculations. We can reasonably assume that DFT is as accurate for the liquid as for the crystal. Then, at this level of accuracy, the comparisons of theory and experiment for the liquid, in Table V, confirm the equations of V-T theory as described in Sec. II. Moreover, confirmation of the equations provides confirmation of the nuclear motion described by the equations. The following discussion adds detail to this secondary conclusion.

In the formula for internal energy, Eq. (2), the major contribution is $\Phi_0^l(V) + U_{\text{vib}}^l(V, T)$. This is a purely theoretical function, and describes normal-mode vibrational motion of the nuclei. Also in Eq. (2), no significant error is contributed by the small terms $U_{\text{tr}}^l(V, T)$ and $U_{\text{el}}^l(V, T)$. Agreement of theory and experiment for the internal energy for one liquid demonstrates consistency of the vibrational motion with experiment. The same argument applies to the liquid entropy, Eq. (3), where the same nuclear motion is described by the purely theoretical function $S_{\text{vib}}^l(V, T)$. Agreement of theory and experiment for the entropy for one liquid demonstrates consistency of the vibrational motion with experiment. Further, the quantities calculated by DFT, $\Phi_0^l(V)$ for the internal energy and $\theta_0^l(V)$ for the entropy, are not theoretically related, so the confirmations obtained from internal energy and entropy are independent.

This situation is analogous when one compares theory with experiment for the liquid volume and bulk modulus. The theoretical functions tested are volume derivatives of $\Phi_0^l(V)$ and $\theta_0^l(V)$, and the comparison with experiment for V_m^l and $B(V_m^l, T_m)$ are independent tests.

Altogether in Table V, four independent consistency tests of the nuclear motion are provided for each of two elemental liquids. The agreement of theory and experiment within small errors for all these tests provides the following two-part verification of V-T theory (for Na and Cu): (a) Many-body harmonic vibrational motion described by the parameters $\Phi_0^l(V)$ and $\theta_0^l(V)$ is the dominant contribution to the thermodynamic functions, and (b) While the experimental liquid moves rapidly among

all the valleys in the potential energy surface, a single random valley at each volume serves to calculate the vibrational motion and its contribution to thermodynamics.

Appendix A: Statistical mechanics for a single potential energy valley

The system has N atoms in a volume V at temperature T , and is confined to a single harmonic potential valley. The system potential energy at the valley minimum, the structure, is $\Phi_0(V)$. The normal mode vibrational frequencies are $\omega_\lambda(V)$ for $\lambda = 4, \dots, 3N$, where the three translational modes are omitted from statistical mechanics. The Helmholtz free energy is F , given by

$$F(V, T) = \Phi_0(V) + F_{\text{vib}}(V, T), \quad (\text{A1})$$

$$F_{\text{vib}}(V, T) = \sum_{\lambda} \left[\frac{1}{2} \hbar \omega_{\lambda} - k_B T \ln(n_{\lambda} + 1) \right], \quad (\text{A2})$$

where n_{λ} is the Bose-Einstein distribution function. In low- and high- T regimes, F_{vib} depends on only a few characteristic temperatures θ_n , which are related to moments of the frequency distribution. Here the important θ_n are given by

$$\ln(k_B \theta_0) = \langle \ln(\hbar \omega) \rangle, \quad (\text{A3})$$

$$k_B \theta_1 = \frac{4}{3} \langle \hbar \omega \rangle, \quad (\text{A4})$$

$$k_B \theta_2 = \sqrt{\frac{5}{3} \langle (\hbar \omega)^2 \rangle}, \quad (\text{A5})$$

where the average $\langle \dots \rangle$ is over the vibrational frequencies.

Functions useful for comparing with experimental data are the internal energy $U(V, T)$, and the entropy $S(V, T)$. These are obtained from the free energy, and Eq. (A1) yields

$$S(V, T) = S_{\text{vib}}(V, T), \quad (\text{A6})$$

$$U(V, T) = \Phi_0(V) + U_{\text{vib}}(V, T). \quad (\text{A7})$$

We shall be interested in the vibrational contributions only at $T = 0$ and T_m . At $T = 0$,

$$S_{\text{vib}}(V, T = 0) = 0, \quad (\text{A8})$$

$$U_{\text{vib}}(V, T = 0) = \frac{9}{8} N k_B \theta_1(V). \quad (\text{A9})$$

The right side of Eq. (A9) is just the harmonic zero-point energy. This equation will be needed below to evaluate the thermodynamic zero of energy. For most monatomic crystals and liquids, the nuclear motion is nearly classical at $T \gtrsim T_m$, and a high- T expansion of n_{λ} in Eq. (A2) is valid. This expansion gives

$$S_{\text{vib}}(V, T) = 3Nk_B \left[\ln \left(\frac{T}{\theta_0(V)} \right) + 1 \right]$$

$$+\frac{1}{40}\left(\frac{\theta_2(V)}{T}\right)^2+\dots\Big], \quad (\text{A10})$$

$$U_{\text{vib}}(V, T) = 3Nk_B T \left[1 + \frac{1}{20} \left(\frac{\theta_2(V)}{T} \right)^2 + \dots \right]. \quad (\text{A11})$$

The series starting with $(\theta_2/T)^2$ expresses the quantum corrections, and only this leading term is required in the present study.

Appendix B: Normalizing DFT energies for thermodynamics

To evaluate the functions in Appendix A, we require the potential energy at the valley minimum $\Phi_0(V)$ and the moments of the vibrational spectrum θ_n for $n = 0, 1, 2$. Extraction of the moments from DFT is described in Sec. II; $\Phi_0(V)$ is determined as follows.

All system energies are to be measured from the thermodynamic zero of energy, which is the energy of the crystal at $T = 0$ and $P = 0$. Here P is pressure, given by $P = -(\partial F/\partial V)_T$. At $T = 0$, the crystal free energy is

$$F^c(V) = U^c(V) = \Phi_0^c(V) + \frac{9}{8}Nk_B\theta_1^c(V). \quad (\text{B1})$$

DFT calculations provide total energies $E(V)$ measured with respect to isolated atoms. To correct the $E(V)$ to the thermodynamic energy zero, we denote the DFT crystal structure energy by $E^c(V)$, and define the constant D by

$$\Phi_0^c(V) = E^c(V) + D. \quad (\text{B2})$$

If V_{ref}^c is the crystal volume at $T = 0$ and $P = 0$, then by definition $U^c(V_{\text{ref}}^c, T = 0) = 0$. Equations (B1) and (B2) can be solved for D to find

$$D = - \left[E^c(V_{\text{ref}}^c) + \frac{9}{8}Nk_B\theta_1^c(V_{\text{ref}}^c) \right]. \quad (\text{B3})$$

Equations (B2) and (B3) define $\Phi_0^c(V)$ in terms of quantities calculated by DFT. To observe the thermodynamic energy zero for a given atomic system, the same D is added to every energy calculated in DFT, for every condensed matter phase, at all V . With this, only DFT energy differences enter the quantities we need to calculate.

As for the crystal valley, potential energy properties of random valleys depend on the system volume. Hence to include volume dependence, a representative random valley is required at a range of volumes. Equation (B2) holds for the liquid, i.e. for each random valley in the form

$$\Phi_0^l(V) = E^l(V) + D. \quad (\text{B4})$$

Acknowledgments

We would like to thank the Ten Bar Café for its impeccable service and highly stimulating beverages. NB would like to thank Matt Challacombe for helpful discussions. This work was supported by the U. S. Department of Energy under Contract No. DE-AC52-06NA25396. EH and RL also acknowledge support from FONDECYT projects 11070115 and 11080259, DID (UACH) grants SR-2008-0 and S-2008-51.

-
- [1] M. Born and K. Huang, *Dynamical Theory of Crystal Lattices* (Oxford University Press, 1998).
- [2] M. C. Payne, M. P. Teter, D. C. Allan, T. A. Arias, and J. D. Joannopoulos, *Rev. Mod. Phys.* **64**, 1045 (1992).
- [3] G. Kresse and J. Hafner, *Phys. Rev. B* **47**, 558 (1993).
- [4] G. A. de Wijs, G. Kresse, and M. J. Gillan, *Phys. Rev. B* **57**, 8223 (1998).
- [5] D. Alfè, G. Kresse, and M. J. Gillan, *Phys. Rev. B* **61**, 132 (2000).
- [6] D. Alfè, G. D. Price, and M. J. Gillan, *Phys. Rev. B* **65**, 165118 (2002).
- [7] J.-D. Chai, D. Stroud, J. Hafner, and G. Kresse, *Phys. Rev. B* **67**, 104205 (2003).
- [8] D. C. Wallace, *Phys. Rev. E* **56**, 4179 (1997).
- [9] E. D. Chisolm and D. C. Wallace, *J. Phys.: Condens. Matter* **13**, R739 (2001).
- [10] E. Holmström, N. Bock, T. B. Peery, R. Lizárraga, G. De Lorenzi-Venneri, E. D. Chisolm, and D. C. Wallace, *Phys. Rev. E* **80**, 051111 (2009).
- [11] E. Holmström, N. Bock, T. Peery, E. Chisolm, R. Lizárraga, G. De Lorenzi-Venneri, and D. Wallace, *Phys. Rev. B* **82**, 024203 (2010).
- [12] D. C. Wallace, E. D. Chisolm, N. Bock, and G. De Lorenzi-Venneri, *Phys. Rev. E* **81**, 041201 (2010).
- [13] G. De Lorenzi-Venneri, E. D. Chisolm, and D. C. Wallace, *Phys. Rev. E* **78**, 041205 (2008).
- [14] D. C. Wallace, E. D. Chisolm, and N. Bock, *Phys. Rev. E* **79**, 051201 (2009).
- [15] Vienna *Ab-initio* Simulation Package (VASP), URL <http://cms.mpi.univie.ac.at/vasp/>.
- [16] P. E. Blöchl, *Phys. Rev. B* **50**, 17953 (1994).
- [17] G. Kresse and D. Joubert, *Phys. Rev. B* **59**, 1758 (1999).
- [18] H. J. Monkhorst and J. D. Pack, *Phys. Rev. B* **13**, 5188 (1976).
- [19] B. E. Clements and D. C. Wallace, *Phys. Rev. E* **59**, 2955 (1999).
- [20] G. De Lorenzi-Venneri and D. C. Wallace, *Phys. Rev. E* **76**, 041203 (2007).
- [21] H. Schober, P. H. Dederichs, and D. J. Sellmeyer, *Phonon States of Elements, Electron States and Fermi Surfaces of Alloys*, vol. 13a (Springer-Verlag, Berlin, 1981).
- [22] N. W. Ashcroft and N. D. Mermin, *Solid State Physics*

- (Brooks Cole, Belmont, 1976), 1st ed.
- [23] P. Vinet, J. Ferrante, J. R. Smith, and J. H. Rose, *Journal of Physics C: Solid State Physics* **19**, L467 (1986).
- [24] D. C. Wallace, *Statistical Physics of Crystals and Liquids: A Guide to Highly Accurate Equations of State* (World Scientific, New Jersey, 2003).
- [25] O. Eriksson, J. M. Wills, and D. C. Wallace, *Phys. Rev. B* **46**, 5221 (1992).
- [26] M. S. Anderson and C. A. Swenson, *Phys. Rev. B* **28**, 5395 (1983).
- [27] M. S. Anderson and C. A. Swenson, *Phys. Rev. B* **31**, 668 (1985).
- [28] M. E. Diederich and J. Trivisonno, *J. Phys. Chem. Solids* **27**, 637 (1966).
- [29] R. H. Martinson, *Phys. Rev.* **178**, 902 (1969).
- [30] G. Simmons and H. Wang, *Single Crystal Elastic Constants and Calculated Aggregate Properties. A Handbook* (MIT Press, Cambridge, 1971), 2nd ed.
- [31] N. Bock, D. Coffey, and D. C. Wallace, *Phys. Rev. B* **72**, 155120 (2005).
- [32] N. Bock, D. C. Wallace, and D. Coffey, *Phys. Rev. B* **73**, 075114 (2006).
- [33] G. Fritsch, F. Geipel, and A. Prasetyo, *J. Phys. Chem. Solids* **34**, 1961 (1973).
- [34] R. Hultgren, P. D. Desai, D. T. Hawkins, M. Gleiser, and K. K. Kelley, *Selected Values of the Thermodynamic Properties of the Elements* (American Society for Metals, Materials Park, Ohio, 1973).
- [35] Y. S. Trelin, I. N. Vasiliev, V. B. Proskurin, and T. A. Tsyganova, *High Temp.* **4**, 352 (1966).
- [36] G. H. Shaw and D. A. Caldwell, *Phys. Rev. B* **32**, 7937 (1985).
- [37] T. Iida and R. I. L. Guthrie, *The Physical Properties of Liquid Metals* (Oxford University Press, USA, 1993).